American Mineralogist, Volume 88, pages 1402–1407, 2003

Structural systematics of hydrous ringwoodite and water in Earth's interior

JOSEPH R. SMYTH,[1,*] CHRISTOPHER M. HOLL,[1] DANIEL J. FROST,[2] STEVEN D. JACOBSEN,[2] FALKO LANGENHORST,[2] AND CATHERINE A. MCCAMMON[2]

[1]Department of Geological Sciences, University of Colorado, Boulder, Colorado 80309, U.S.A.
[2]Bayerisches Geoinstitut, Universität Bayreuth, Bayreuth D95440, Germany

ABSTRACT

Seven separate samples of hydrous ringwoodite with compositions ranging from Fo_{100} to Fo_{89} and hydrogen contents from 0.2 to 1.1 wt% were synthesized in the 5000 ton multi-anvil press at the Bayerisches Geoinstitut. Synthesis conditions ranged from 18 to 22 GPa and 1400 to 1500 °C. The crystals were characterized by single-crystal X-ray diffraction, electron microprobe, IR and Mössbauer spectroscopy, and by analytical and high-resolution transmission electron microscopy. The crystals are optically isotropic, and the Fe-bearing samples are deep blue in color. Mössbauer spectroscopy and ELNE spectroscopy applied to the Fe-bearing samples indicates about 10% of the iron is in the ferric state. High-resolution TEM examination of one of the Fe-bearing samples indicates that the crystals are homogeneous and free of significant inclusions or exsolution features. Infrared spectra show a broad absorption band extending from about 2500 to 3600 cm^{-1} with maxima ranging from 3105 for the pure magnesian samples to 3150 cm^{-1} for the Fo_{89} samples. The crystal structures of the seven ringwoodite samples were refined by X-ray single-crystal diffraction. Refinement of cation site occupancies indicates full occupancy of the tetrahedral site for all samples, whereas the occupancy of the octahedral site appears to decrease systematically with H content. The principal hydration mechanism involves octahedral cation vacancies. The IR spectra are consistent with protonation of the short O-O approach on the tetrahedral edge, which would imply partial Mg-Si disorder.

INTRODUCTION

Earth is distinguished from its planetary neighbors by the presence of large amounts of liquid water on its surface. Sea level variation studies indicate that sea level has varied relatively little, at least throughout the Phanerozoic. The presence of quartz-pebble conglomerates of early Archean age indicates that there has been running water (implying the presence of both oceans and land) nearly as far back as we can see in geologic time. Recent geochemical studies of ancient zircons by Mojzsis et al. (2001) indicate that there may have been liquid water as far back as 4.3 GY ago. Although the oceans cover 72% of the surface area, they constitute only 0.025% of the planet's mass. Silicate minerals of the crust and upper mantle can incorporate many times this amount of water, so it is likely that these minerals have played a major role in maintaining Earth's oceans over geologic time.

Approximately 65% of the mass of the planet is composed of silicate rocks of the mantle and crust in which the only significant anionic species is O atoms. Bulk hydrogen content is perhaps the most poorly constrained compositional variable in the planet, and the total water content of the planet is unknown within an order of magnitude. The nominally anhydrous silicate minerals that compose the upper 660 km of the Earth are likely to constitute the planet's largest reservoir of water. Olivine, generally believed to be the most abundant mineral phase in the upper 400 km, can incorporate up to 2000 ppm by weight H_2O (Kohlstedt et al. 1996) at 13 GPa and 1100 °C. The maximum water content of pyroxenes is not known, but natural clinopyroxenes have been reported with up to about 1800 ppm OH (Rossman and Smyth 1990; Smyth et al. 1991). In the Transition Zone (410–660 km), wadsleyite (β-Mg_2SiO_4) can incorporate up to about 3.3 wt% H_2O, (Kohlstedt et al. 1996; Inoue et al. 1995), and ringwoodite (γ-Mg_2SiO_4) has been reported with up to about 2.2 wt% H_2O (Kohlstedt et al. 1996; Kudoh et al. 2000).

Smyth (1987, 1994) predicted that wadsleyite might contain significant amounts of H_2O based on the anomalous bonding around the O1 atom, which is undersaturated and has a very shallow electrostatic site potential. However, the O atom coordination in ringwoodite is similar to olivine in that each O atom is bonded to three octahedral divalent cations and one tetrahedral tetravalent cation. There is no obvious reason then that ringwoodite should incorporate such large amounts of water. Kudoh et al. (2000) report an X-ray crystal structure determination of hydrous, pure Mg ringwoodite, but did not report a proton position. They did report significant cation site vacancies and some relatively small amounts of Mg-Si disorder. In order to confirm these findings and gain a better understanding of silicate spinels in the planet's water budget, we have undertaken an experimental study of hydrous silicate spinels. We have synthesized hydrous ringwoodite of pure magnesian and likely mantle compositions, and determined the

* E-mail: joseph.smyth@colorado.edu

0003-004X/03/0010–1402$05.00

mechanisms of hydration by means of X-ray single crystal diffraction, transmission electron microscopy (TEM), and infrared (IR) spectroscopy. The crystal size is relatively large (100 to 800 μm), and samples from this study are available for further investigations. In addition to the characterization and structural studies described here, Kleppe et al. (2002a, 2002b) have described the Raman spectra to pressures above 50 GPa, Kavner and Duffy (2000) have studied the deformation strength of one of the samples, and gigahertz ultrasonic measurements are in progress.

EXPERIMENTAL METHODS

Synthesis

The starting materials for the Fe-bearing compositions were made up of natural Fo_{90} olivine, En_{90} orthopyroxene, plus brucite, hematite, and silica to give a bulk water content of 3 wt%. The starting material for the Fe-free samples was a mixture of MgO, brucite, and silica to give a composition of Mg_2SiO_4 plus 4 wt% H_2O. The starting materials were sealed in a welded Pt capsule approximately 2 mm in diameter by 3.5 mm in length. The experimental conditions and phase assemblages are outlined in Table 1. The 5000 ton press at the Bayerisches Geoinstitut was used to compress the octahedra using 52 mm edge-length WC anvils with 11 mm corner truncations. A Cr_2O_3-doped MgO multi-anvil octahedron of 18 mm edge-length was employed with a stepped lanthanum chromate heater. The capsules were placed into the assembly inside a sintered MgO sleeve. The heating time for each experiment was nominally five hours. The temperature was monitored and controlled to within 1 °C during the experiments using a W3%Re/W25%Re thermocouple that was inserted axially into the assembly.

Chemical analysis

The ringwoodite crystals were first analyzed by electron microprobe; their compositions are given in Table 2. Mössbauer spectroscopy was performed on samples SZ9901 and SZ0002 to determine the relative concentration of Fe^{3+}. Spectra were collected at room temperature using the milliprobe method (McCammon et al. 1991; McCammon 1994) and indicated $Fe^{3+}/\Sigma Fe$ values of approximately 10% for both samples. The same values were assumed for samples SZ0104 and SZ0107 for calculation of cation ratios in Table 2.

Infrared spectra were used to estimate the H contents of these samples. Spectra were measured using a Thermo-Nicolet 670 FTIR spectrometer with microscope. Samples were prepared as randomly oriented double-polished single crystals on a 2 mm NaCl single crystal substrate. Sample thickness was measured using a Mitutoyo digital micrometer and ranged from 24 to 56 μm. Spectra were measured from clear areas of the crystals devoid of obvious fractures or inclusions. Sample areas were approximately 50× 50 μm square. Details of the IR experiments are given in Table 3 and typical spectra from the 2500 to 4000 cm^{-1} region are given in Figure 1.

The O-H absorption appears as a very broad band from about 2500 to 3800 cm^{-1}, with the largest absorbance peak at about 3105 cm^{-1} for the Fe-free samples and at about 3140 cm^{-1} for the Fe-bearing samples. The observed spectra are highly reproducible from different areas of each grain and from grain to grain within each experiment. The spectra were corrected for thickness and the absorption in the region of 3780 to 2605 cm^{-1} was integrated for each spectrum. Using the calibration of Kohlstedt et al. (1996) we estimated the hydroxide content of each sample and these data are reported as wt% H_2O in Table 2.

Transmission electron microscopy

To test for possible defects or precipitates, we studied one ringwoodite grain (SZ9901) with analytical transmission electron microscopy (Philips CM20 STEM). The grain was first crushed; its fragments were dispersed in a droplet of ethanol and then loaded on a holey carbon grid. Under the TEM, the ringwoodite fragments are essentially free of defects or hydrous precipitates. We particularly note the absence of stacking faults, which are commonly observed on {110} planes of meteoritic ringwoodite (Langenhorst et al. 1995). The perfection of the crystal lattice is also obvious from high-resolution TEM images (Fig. 2), which reveal a regularly spaced lattice. The only defects observed are few dislocations. The dislocation density is heterogeneous and quite low, less than 10^8 dislocations per cm^2 in regions where dislocations can be observed at all.

In addition to the microstructural observations, we used a parallel electron energy loss spectrometer (Gatan PEELS 666) to measure the Fe L_{23} electron-energy loss near-edge structure (ELNES) of ringwoodite, which is a quantitative measure of the ferric/ferrous ratio (van Aken et al. 1998). ELNES spectra were acquired at three different places on the ringwoodite sample with an en-

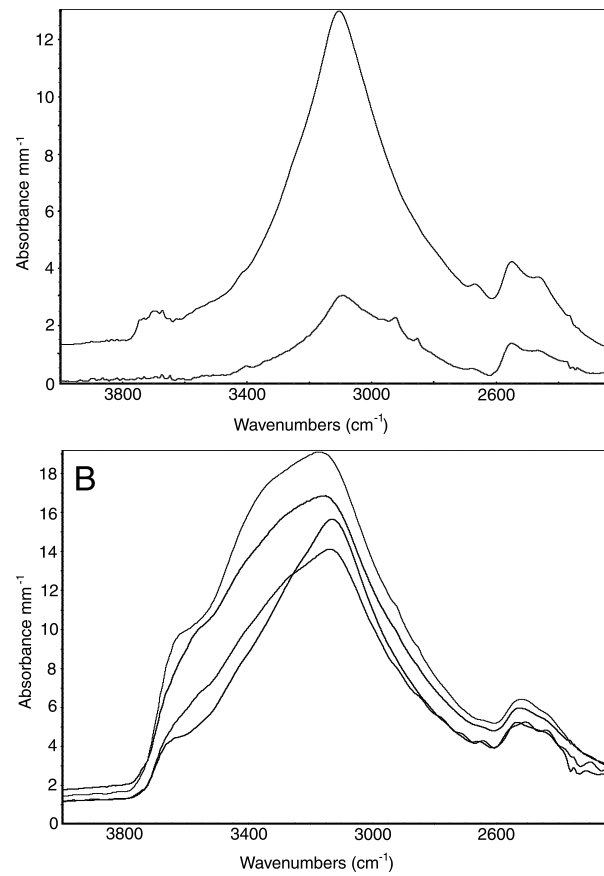

FIGURE 1. Infrared spectra of ringwoodite samples in absorbance per mm vs. wavenumbers. (**a**) Two Fo_{100} ringwoodite samples. (**b**) Four $Fo_{88\text{-}90}$ ringwoodite samples.

TABLE 1. Ringwoodite synthesis conditions

Sample	Ringby4	Ringby2	Ringby5	SZ0107	SZ0002	SZ9901	SZ0104
Temperature (°C)	1500	1500	1500	1400	1400	1400	1400
Pressure	21	22	21.5	19.0	20.0	20.0	18
Phase assemblage							
Ringwoodite	100	100	100	85	85	85	80
Wadsleyite	0	0	0	10	0	0	10
Garnet	0	0	0	5	0	0	5
Stishovite	0	0	0	0	10	10	0
Quench	0	0	0	5	5	5	5

TABLE 2. Chemical analyses of seven ringwoodites based on electron microprobe, IR, and Mössbauer spectroscopy

Sample	Ringby4	Ringby2	Ringby5	SZ0107	SZ0002	SZ9901	SZ0104
				Weight percent oxides			
SiO_2	42.80	42.60	42.60	41.19	40.87	39.92	40.92
TiO_2	0.00	0.00	0.00	0.02	0.02	0.02	0.02
Al_2O_3	0.00	0.00	0.00	0.07	0.09	0.14	0.16
Cr_2O_3	0.00	0.00	0.00	0.02	0.04	0.07	0.06
Fe_2O_3	0.00	0.00	0.00	1.03	1.06	1.23	1.42
FeO	0.00	0.00	0.00	9.33	9.52	10.00	11.30
MnO	0.00	0.00	0.00	0.04	0.04	0.05	0.05
MgO	57.00	56.50	56.50	48.10	46.40	45.89	44.87
CaO	0.00	0.00	0.00	0.00	0.02	0.02	0.02
Na_2O	0.00	0.00	0.00	0.00	0.00	0.00	0.00
K_2O	0.00	0.00	0.00	0.00	0.00	0.00	0.00
H_2O	0.20	0.75	0.74	0.86	0.79	0.93	1.07
Total							
				Cations per four O atoms			
Si	1.000	0.991	0.991	0.993	1.003	0.987	0.999
Ti	0.000	0.000	0.000	0.000	0.000	0.000	0.000
Al	0.000	0.000	0.000	0.002	0.003	0.004	0.005
Cr	0.000	0.000	0.000	0.000	0.001	0.001	0.001
Fe^{3+}	0.000	0.000	0.000	0.019	0.020	0.023	0.026
Fe^{2+}	0.000	0.000	0.000	0.188	0.195	0.207	0.231
Mn	0.000	0.000	0.000	0.001	0.001	0.001	0.001
Mg	1.985	1.959	1.960	1.729	1.697	1.696	1.633
Ca	0.000	0.000	0.000	0.000	0.001	0.000	0.001
Na	0.000	0.000	0.000	0.000	0.000	0.000	0.000
K	0.000	0.000	0.000	0.000	0.000	0.000	0.000
yH	0.031	0.116	0.115	0.138	0.129	0.154	0.174

TABLE 3. Estimated H contents from IR spectra

Sample	Rinby4	Ringby2	Ringby5	SZ0107	SZ0002	SZ9901	SZ0104
Peak maximum	3102	3104	3104	3126	3130	3150	3150
Integration	11.00	40.75	40.69	47.35	43.67	51.25	58.99
H_2O ppm wt	1988	7358	7354	8557	7892	9263	10661
$H/10^6Si$	32 300	120 000	119 500	139 000	128 000	150 000	173 000

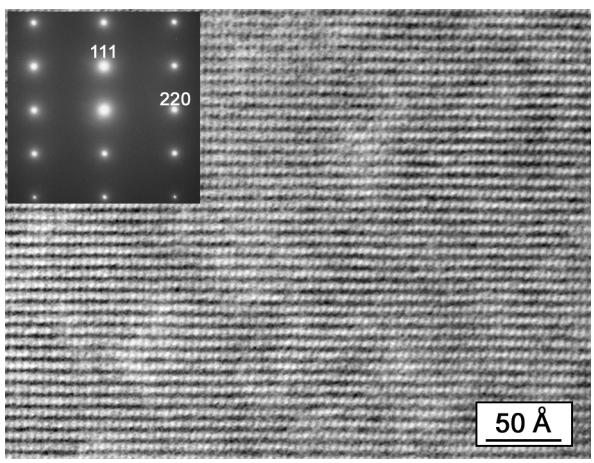

FIGURE 2. High-resolution TEM image and corresponding selected area electron diffraction pattern of ringwoodite SZ9901, taken down the [$\bar{1}$10] zone axis.

ergy dispersion of 0.1 eV per channel. The evaluation of ELNES spectra involved the subtraction of an inverse power law background, the removal of plural scattering contributions by the Fourier-ratio technique, and the subtraction of an arctan function (Frost and Langenhorst 2002). The quantification of ferric/ferrous ratios was then done according to the universal technique (van Aken et al. 1998).

The ELNES data reveals a slight heterogeneity in the ferric content, ranging from 4% to 14% (Fig. 3). The average ferric content is 9%, in good agreement with Mössbauer results.

X-ray diffraction

X-ray diffraction studies were preformed with a Siemens/Bruker P4 automated diffractometer with an 18 kW rotating Mo anode source operating at 50 kV and 250 mA. The diffractometer has a graphite-crystal monochromator diffracting in the horizontal plane. This geometry causes the monochromator to induce small shifts in the proportions of the Mo$K\alpha_1$ and Mo$K\alpha_2$ peaks at low-angles where the two wavelengths are not effectively separated. This requires that the wavelength of the mixed Mo$K\alpha$ peak be calibrated frequently against a known standard. The wavelength of the Mo$K\alpha$ was determined from cell refinement of a standard ruby sphere immediately before and after each cell determination. The unit-cell parameters of the ringwoodite samples were then determined by refinement from the centering angles of 24 or more diffraction peaks in both positive and negative 2θ positions. Cell parameter precisions (Table 4) determined in this manner are generally better than one part in 20 000 and reproducible to about one part in 10 000.

X-ray diffraction intensities were measured using θ-2θ scans and variable scan speeds ranging from 2–10° 2θ per minute. A single octant of reciprocal space was measured for each crystal with maximum 2θ of at least 70°. The data were corrected for Lorenz and polarization effects and for absorption using the analytical absorption correction routine in WinGX32. Equivalent intensities were averaged with an R of merging (R_{int}) ranging from 0.012 to 0.031. Data collection parameters for each sample are given in Table 4.

Atom position and anisotropic displacement parameters, cation occupancy, and isotropic extinction parameters were refined by least-squares of F^2 using SHELXL-97 (Sheldrick 1997). Initial atom positions were for a cubic spinel in space group $Fd3m$ with an assumed O atom position parameter of 0.25. X-ray scattering curves were those of Cromer and Mann (1968) for fully ionized cations and O^{-1}. The scattering of O atoms was fit using a mixture of O^{-1} (Cromer and Mann 1968) and O^{-2} (Tokonami 1965). Cation occupancies of light elements like Si and Mg are sensitive to the scattering curve used for O atoms. For the Fe free samples, the distributed scattering factor for O atoms between O^{-1} and O^{-2} was refined along with the cation occupancies. Each O atom refinement gave very similar results with the average distribution being 75% O^{-2} and 25% O^{-1}. This value was then used and fixed for all refinements and resulted in neg-

TABLE 4. Data for ringwoodite structure refinements

Sample	Ringby4	Ringby2	Ringby5	SZ0107	SZ0002	SZ9901	SZ0104
N_{meas}	840	786	786	1839	759	786	946
N_{unique}	87	87	87	180	88	88	102
R_{int}	0.014	0.026	0.014	0.015	0.012	0.026	0.013
R	0.020	0.028	0.021	0.022	0.016	0.032	0.018
R_w ($F > 4\sigma$)	0.015	0.016	0.014	0.019	0.015	0.020	0.016
A	8.0633(3)	8.0682(5)	8.0687(4)	8.09027(18)	8.0904(4)	8.0944(4)	8.1053(3)
V	524.25(7)	525.21(11)	525.30(8)	529.53(3)	529.55(9)	530.34(9)	532.49(7)
Octahedral site							
Total occ	99.8(9)	97.2(8)	97.3(7)	95.7(5)	97.7(5)	98.1(6)	96.1(6)
Mg occ	99.8(9)	97.2(8)	97.3(7)	85.4(5)	86.9(5)	86.6(6)	83.2(6)
Fe occ	0.0	0.0	0.0	10.3	10.8	11.5	12.9
U_{11}	0.00516(27)	0.00488(35)	0.00556(31)	0.00489(12)	0.00547(24)	0.00548(26)	0.00564(22)
U_{12}	–.00058(13)	–.00032(19)	–.00060(14)	–0.00042(5)	–.00039(13)	–.00045(10)	–.00064(11)
Uso	0.00516(16)	0.00488(20)	0.00561(10)	0.00489(12)	0.00547(14)	0.00548(15)	0.00564(12)
Tetrahedral site							
Si occ (%)	100.8(9)	99.4(8)	100.1(6)	99.5(8)	100.5(8)	101.5(12)	98.7(10)
U_{11} (= U_{iso})	0.00426(14)	0.00405(19)	0.00479(19)	0.00458(13)	0.00590(16)	0.00581(32)	0.00673(23)
O atom site							
X	0.24391(6)	0.24393(10)	0.24377(7)	0.24354(4)	0.24345(7)	0.24328(12)	0.24341(7)
U_{11}	0.00459(31)	0.00475(41)	0.00545(31)	0.00530(15)	0.00601(27)	0.00530(37)	0.00668(37)
U_{12}	–0.00044(20)	–0.00051(26)	–0.00056(20)	–0.00030(8)	–0.00006(19)	–0.00026(33)	0.00002(16)
U_{iso}	0.00459(20)	0.00475(24)	0.00545(31)	0.00530(15)	0.00601(27)	0.00530(37)	0.00668(16)
EXTI	0.0025(12)	0.0020(12)	0.0022(12)	0.0092(17)	0.0000(9)	0.0000(18)	0.0015(10)
Residual 1 (e–)	0.49	0.46	0.50	0.76	0.47	0.58	0.32
x	0.066	0.072	0.189	0.094	0.189	0.072	0.188
y	0.066	0.072	0.189	0.094	0.189	0.072	0.188
z	0.184	0.178	0.189	0.094	0.189	0.178	0.188
Residual 2 (e–)	0.35	0.25	0.31	0.71	0.19	0.52	0.31
x	0.072	0.625	0.073	0.066	0.0	0.625	0.076
y	0.178	0.625	0.177	0.066	0.0	0.625	0.076
z	0.178	0.625	0.177	0.184	0.0	0.625	0.174

Notes: Refinements were done using SHELXL-97. Scattering factors for Mg^{2+}, Fe^{2+}, Si^{4+}, O^{-1}, and O^{2-} were taken from Cromer and Mann (1968) and Tokonami (1965).

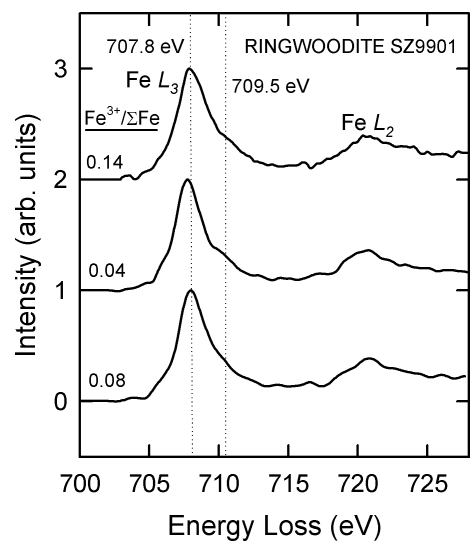

FIGURE 3. Fe L_{23} ELNES spectra taken at three different places on ringwoodite sample SZ9901. The peak at 708.5 eV is indicative of ferrous iron, whereas the peak at 709.5 eV is due to the ferric iron.

ligible change in refined occupancies for the three Fe-free crystals. For the Fe-bearing samples, all of the Fe from the electron microprobe chemical analysis was constrained to be in the octahedral site, and the remaining occupancy was refined as Mg. Final refined parameters are given in Table 4. The converged weighted $R(F)$ for diffractions with intensities greater than 4σ (Table 4) ranged from 0.013 to 0.020. The calculated interatomic distances and polyhedral volumes and distortion parameters are presented in Table 5.

DISCUSSION

Hydroxyl contents derived exclusively from IR spectroscopy may be somewhat controversial. Ringwoodite shows a very broad absorption feature (Fig. 1) associated with O-H stretching motion that might be interpreted as liquid water. However, previous studies of hydration of ringwoodite show similar features (Kudoh et al. 2000; Kohlstedt et al. 1996). In addition, our IR spectra were highly reproducible from grain to grain within an experiment, and as discussed below, show a strong correlation with unit-cell volume. We attempted SIMS analysis for H on a few of these samples, but the results were inconclusive. Very large corrections for decaying counts were required, resulting in large errors and concentrations that were not consistent or reproducible (Hervig, pers. comm.). We therefore used the method reported by Kohlstedt et al. (1996) in which

$$C_{OH} = (B_i / 150\zeta) \int H(\nu) / (3780 - \nu)$$

where C_{OH} is the molar concentration of hydroxyl, $H(\nu)$ is an absorption coefficient in mm^{-1}, ζ is an orientation factor (1/3), and B_i a calibration factor that incorporates the unit-cell volume. As Kohlstedt et al. (1996) caution, these results should be regarded as first-order estimates as absolute concentrations may be in error by as much as 50%. However, reproducibility and relative precision are only a few percent. Results are given in Table 3 and incorporated into the chemical analyses reported in Table 2.

Kohlstedt et al. (1996) and Kudoh et al. (2000) report sig-

TABLE 5. Ringwoodite structure details

Sample	Ringby5	Ringby2	Ringby5	SZ0107	SZ0002	SZ9901	SZ0104
Mg/(Mg + Fe)	100	100	100	89.7	89.2	88.5	87.1
H pfu	0.031	0.116	0.115	0.138	0.129	0.154	0.174
Octahedron							
Total occ	99.8(9)	97.2(8)	97.3(7)	95.7(5)	97.7(5)	98.1(6)	96.1(6)
Mg occ	99.8(9)	97.2(8)	97.3(7)	85.4(5)	86.9(5)	86.6(6)	83.2(6)
Fe occ	0.0	0	0	10.3	10.8	11.5	12.9
Mg-O (Å)	2.0661(6)	2.0673(8)	2.0686(6)	2.0762(4)	2.0769(6)	2.0782(11)	2.0809(6)
Avg. edge length	2.9211(9)	2.9228(12)	2.9245(10)	2.9353(6)	2.9362(10)	2.9385(11)	2.9408(9)
Poly. vol. (Å^3)	11.719	11.740	11.759	11.888	11.897	11.924	11.967
AngVar	7.90	7.87	8.20	8.87	9.06	9.24	9.14
Si occ	100.8(9)	99.4(8)	100.1(6)	99.5(8)	100.5(8)	101.5(12)	98.7(10)
Si-O (Å)	1.6607(6)	1.6619(8)	1.6600(6)	1.6609(4)	1.6600(6)	1.6598(11)	1.6640(6)
Edge length	2.7119(9)	2.7138(12)	2.7110(10)	2.7123(6)	2.7107(10)	2.7105(15)	2.7173(9)
Poly. vol. (Å^3)	2.351	2.354	2.348	2.352	2.347	2.347	2.365
AngVar	0.0	0.0	0.0	0.0	0.0	0.0	0.0

nificantly higher H contents in ringwoodite than observed here, and their IR spectra are qualitatively somewhat different, showing absorption features at 3345 and 3645 cm^{-1} in addition to the feature at 3100–3120 cm^{-1} observed in our spectra. Kudoh et al. (2000) report that the solubility of H in ringwoodite decreases with temperature. The samples studied by Kohlstedt et al. (1996) were synthesized at 1100 °C and that of Kudoh et al. (2000) at 1300 °C, whereas those in the current study were synthesized at 1400 °C. The unit-cell volume reported by Kudoh et al. (2000) is larger than observed here, consistent with a systematic expansion of the cell volume with hydration.

The crystal structure refinements reported in Tables 4 and 5 are of sufficient precision to give a good understanding of the effects of hydration on the crystal structure of ringwoodite. It is clear from the occupancy refinements of both Fe-free and Fe-bearing samples that the principal mechanism of hydration is octahedral cation vacancy. All samples show full occupancy of the tetrahedral sites within 1.5 σ. Kudoh et al. (2000) reported cation vacancies at both sites. The least hydrous sample shows essentially full occupancy of the octahedral site as well. However, the six hydrous samples show less than full occupancy of the octahedral site, and we observe a good correlation of refined octahedral site occupancy with H contents. The occupancy parameters refined from the X-ray data are consistent with the electron microprobe data in showing a deficiency of divalent cations relative to Si for the hydrous samples. Examining the site polyhedral volume, we observe a slight expansion of the octahedral site, but not the tetrahedral site, with increasing H content (Table 5). We can therefore conclude with high confidence that the principal mechanism for hydration of ringwoodite is octahedral site vacancy. Kudoh et al. (2000) report cation vacancies at both octahedral and tetrahedral sites with octahedral vacancies predominating, however their sample contained significantly more H.

Both Kudoh et al. (2000) and Hazen et al. (1993) report small amounts of cation disorder in pure-Mg ringwoodite. This is very difficult to determine with confidence from X-ray diffraction data because of the close similarity in scattering of Si^{4+} and Mg^{2+} and the possibility of vacancies at both sites. Furthermore, the refined cation occupancies are somewhat dependent on the scattering curve used for O atoms. Hazen et al. (1993) did not recognize the possibility of significant hydration of ringwoodite and so did not report an H content for their sample. Given the possibility of cation vacancies, it seems likely (in retrospect) that the sample studied by Hazen et al. (1993) contained significant amounts of hydroxyl. They report a relatively large unit-cell volume, which is more likely due to hydration than to cation disorder. We can use our unit-cell data as a function of H content for the pure Mg ringwoodites to obtain a hypothetical cell parameter for H-free Mg ringwoodite. As illustrated in Figure 4, we obtain a cell volume of 523.9(1) Å^3 and a cell edge of 8.0615(8) Å for completely anhydrous ringwoodite, if we use only the current data, and 524.1(1) Å^3 and 8.0625 Å if we include the data point of Kudoh et al. (2000). The cell volume reported by Hazen et al. (1993) is interpreted on this curve, and as shown the indicated water content is about 1.5 wt%.

The refinements reported in Table 4 are of relatively high precision, so it is of interest to examine the residua in the difference-Fourier maps to look for site disorder or possible proton positions. The two largest residua in each refinement are listed in Table 4 as height (electrons) and position in fractional coordinates. Difference map residua can result from many causes other than actual excess electron density. They can result from errors in absorption correction or other correction procedures or other systematic errors, but consistently observed residua in several structures at reasonable interatomic distances may be significant. In two of the structures, we observe partial occupancy of a normally vacant tetrahedral site at (5/8, 5/8, 5/8). A one-half electron at this position would be equivalent to about 5% occupancy of this site by Si or Mg. One of the structures (SZ0002) shows a small residual at a normally vacant octahedral site at (0, 0, 0). In every structure we observe electron density residua in the occupied tetrahedral site, either along the Si-O bond near (0.07, 0.07, 0.18), or on the tetrahedral edge near (0.08, 0.18, 0.18). The latter is a possible proton position if hydration occurs on the short O-O approach on the tetrahedral edge.

Libowitzky (1999) reported a strong correlation between O-O distance and O-H stretching frequency as observed in IR spectra for a host of compounds. The absorption feature near 3105 cm^{-1} would correlate with an O-O distance of about 2.7 Å. The tetrahedral edge in this structure is 2.71 Å long (Table 5), whereas the edge lengths of the octahedron are 2.86 and 3.01 Å. Interestingly, the additional features observed the IR and Raman spectra of the samples of Kudoh et al. (2000) and Kohlstedt et al. (1996) would correspond to protonation of the octahedral edge as well as the tetrahedral edge. Furthermore,

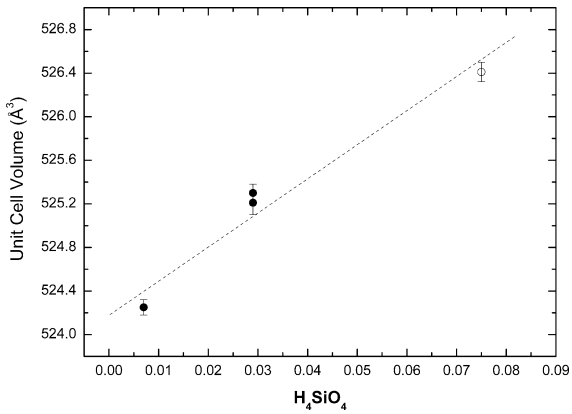

FIGURE 4. Plot of unit-cell volume of Fe-free ringwoodite vs. mole fraction of H_4SiO_4 from this study (solid symbols) and Kudoh et al. (2000) (open symbol).

the most hydrous of the current samples show additional IR absorptions near 3500 cm^{-1} (Fig. 1), consistent with small partial protonation of the octahedral edge. Dominant protonation of the shorter tetrahedral edge in light of the nearly full occupancy of the tetrahedral site would imply partial occupancy of the tetrahedral site by Mg, that is, cation disorder.

Partial occupancy of normally vacant tetrahedral voids has been observed in both hydrous wadsleyite (Smyth et al. 1997) and hydrous wadsleyite II (Smyth and Kawamoto 1997). Occupancy of adjacent tetrahedral voids in the spinel structure would create an Si_2O_7 group with a bridging O atom which would require a non-silicate O atom elsewhere. Also, Kleppe et al. (2002b) report Raman spectra of these hydrous ringwoodite samples at pressures above 50 GPa (i.e., above the stability field of ringwoodite) in which they see evidence of reversible movement of Si from tetrahedral to octahedral coordination.

In conclusion, we report high precision crystal structure refinements of seven ringwoodite samples with various H and Fe contents synthesized at 1400–1500 °C at pressures of 18–22 GPa. IR spectra indicate that the H_2O contents range from 0.2–1.1 wt% H_2O, and microprobe chemical analysis indicates that Mg/(Fe + Mg) compositions range from 1.00 to 0.89. We observe a consistent volume expansion of the structure, both the unit-cell volume and the octahedral site volume with H content as well as occupancy defficiencies at the octahedral site, indicating that octahedral site vacancy is associated with hydration. Tetrahedral sites are nearly full, and volumes appear to be nearly constant over the composition range. Infrared specta are consistent with protonation of the tetrahedral edge as are electron density residua in the X-ray crystal structure refinements. This would require up to about 5% cation disorder of Mg into the tetrahedral site, consistent with previous studies. A plot of unit-cell volume vs. mole fraction of the H_4SiO_4 spinel end-member is consistent with previous studies and indicates a H-free pure Mg_2SiO_4 cell volume of 524.0(2) Å^3 and cell edge of 8.062(1) Å. It appears that H solubility in ringwoodite decreases with temperature and although ringwoodite may be a major host for H and thus water in the Transition Zone, it would be capable of incorporating less water than wadsleyite on a typical geotherm.

Our principal objective in this study has been to syntheisize and characterize a suite of hydrous ringwoodite samples for future quantitative measurements of physical and mechanical properties that may provide a better constraint on the bulk hydrogen content of the Earth.

ACKNOWLEDGMENTS

This work was directly supported by NSF grant EAR 0087279 to J.R.S. and by the Bayerisches Geoinstitut Visitor Program.

REFERENCES CITED

Cromer, D.T. and Mann, J. (1968) X-ray scattering factors computed from numerical Hartree-Fock wave functions. Acta Crystallographica, A24, 321–325.

Frost, D.J. and Langenhorst, F. (2002) The effect of Al_2O_3 on Fe-Mg partitioning between magnesiowüstite and magnesium silicate perovskite. Earth and Planetary Science Letters, 199, 227–241.

Hazen, R.M., Downs, R.T., Finger, L.W., and Ko, J. (1993) Crystal chemistry of ferromagnesian silicate spinels: evidence for Mg-Si disorder. American Mineralogist, 78, 1320–1323.

Inoue, T., Yurimoto, H., and Kudoh, Y. (1995) Hydrous modified spinel, $Mg_{1.75}SiH_{0.5}O_4$: a new water reservoir in the mantle transition region. Geophysical Research Letters, 22, 117–120.

Kavner, A. and Duffy, T.N. (2000) The strength of a natural ringwoodite at transition zone pressures. Eos Transactions. AGU, 81 (48), Fall Meet. Suppl., Abstract T71B–01.

Kleppe, A.K., Jephcoat, A.P., and Smyth, J.R. (2002a) Raman spectra of hydrous ringwoodite γ-Mg_2SiO_4 to 60 GPa. Physics and Chemistry of Minerals, 29, 473–476.

Kleppe, A.K., Jephcoat, A.P., Smyth, J.R., and Frost, D.J. (2002b) On protons, iron, and the high pressure behaviour of ringwoodite. Geophysical Research Letters, 29, DOI:10.1029/2002GL015276.

Kohlstedt, D.L., Keppler, H., and Rubie, D.C. (1996) The solubility of water in α, β and γ phases of $(Mg,Fe)_2SiO_4$. Contributions to Mineralogy and Petrology, 123, 345–357.

Kudoh, Y., Kuribayashi, T., Mizohata, H., and Ohtani, E. (2000) Structure and cation disorder of hydrous ringwoodite, γ-$Mg_{1.89}Si_{0.97}H_{0.34}O_4$. Physics and Chemistry of Minerals, 27, 474–479.

Langenhorst, F., Joreau, P., and Doukhan, J.-C. (1995) Thermal and shock metamorphism of the Tenham chondrite: A TEM examination. Geochimica et Cosmochimica Acta, 59, 1835–1845.

Libowitzky, E. (1999) Correlation of O-H stretching frequencies and O-H∞∞∞∞O hydrogen bond lengths in minerals. Monatshefte für Chemie, 130, 1047–1059.

McCammon, C.A. (1994) A Mössbauer milliprobe: Practical considerations. Hyperfine Interactions, 92, 1235–1239.

McCammon, C.A., Chaskar, V., and Richards, G.G. (1991) A technique for spatially resolved Mössbauer spectroscopy applied to quenched metallurgical slags. Measurement Science and Technology, 2, 657–662.

Mojzsis, S.J., Harrison, T.M., and Pidgeon, R.T. (2001) Oxygen isotope evidenc4e from ancient zircons for liquid water at the Earth's surface 4,300 Myr ago. Nature, 409, 178–181.

Rossman, G.R. and Smyth, J.R. (1990) Hydroxyl and ammonia contents of accessory minerals in mantle eclogites and related rocks. American Mineralogist, 75, 775–780.

Sheldrick, G.M. (1997) SHELXL-97 A program for crystal structure refinement. University of Goettingen, Germany, Release 97–2.

Smyth, J.R. (1987) Beta-Mg_2SiO_4: a potential host for water in the mantle? American Mineralogist, 72, 1051–1055.

——— (1994) A crystallographic model for hydrous wadsleyite (β-Mg_2SiO_4): An ocean in the Earth's interior? American Mineralogist, 79, 1021–1025.

Smyth, J.R. and Kawamoto, T. (1997) Wadsleyite II: a new high pressure hydrous phase in the peridotite-H_2O system. Earth and Planetary Science Letters, 146, E9–E16.

Smyth, J.R., Bell, D.R., and Rossman, G.R (1991) Hydrous clinopyroxenes from the upper mantle. Nature, 351, 732–735.

Smyth, J.R., Kawamoto, T., Jacobsen, S.D., Swope, R.J., Hervig, R.L., and Holloway, J.R. (1997) Crystal structure of monoclinic hydrous wadsleyite. American Mineralogist, 82, 270–275.

Tokonami, M. (1965) Atomic scattering factor for O^{2-}. Acta Crystallographica, 19, 486.

van Aken, P.A., Liebscher, B., and Styrsa, V.S. (1998) Quantitative determination of iron oxidation states in minerals using Fe $L_{2,3}$-edge electron energy-loss near-edge spectroscopy. Physics and Chemistry of Minerals, 5, 323–327.

MANUSCRIPT RECEIVED AUGUST 24, 2002
MANUSCRIPT ACCEPTED DECEMBER 27, 2002
MANUSCRIPT HANDLED BY GEORGE LAGER